

# Effects of ambient hydrostatic pressure on the material properties of the encapsulation of an ultrasound contrast microbubble

Krishna N. Kumar and Kausik Sarkar<sup>a)</sup>

Department of Mechanical and Aerospace Engineering, The George Washington University, Washington, DC 20052, USA

(Received 9 December 2014; revised 15 June 2015; accepted 20 June 2015; published online 6 August 2015)

Ultrasound contrast microbubbles experience widely varying ambient blood pressure in different organs, which can also change due to diseases. Pressure change can alter the material properties of the encapsulation of these microbubbles. Here the characteristic rheological parameters of contrast agent Definity are determined by varying the ambient pressure (in a physiologically relevant range 0–200 mm Hg). Four different interfacial rheological models are used to characterize the microbubbles. Effects of gas diffusion under excess ambient pressure are investigated in detail accounting for size decrease of contrast microbubbles. Definity contrast agent show a change in their interfacial dilatational viscosity ( $3.6 \times 10^{-8}$  Ns/m at 0 mm Hg to  $4.45 \times 10^{-8}$  Ns/m at 200 mm Hg) and interfacial dilatational elasticity (0.86 N/m at 0 mm Hg to 1.06 N/m at 200 mm Hg) with ambient pressure increase. The increase results from material consolidation, similar to such enhancement in bulk properties under pressure. The model that accounts for enhancement in material properties with increasing ambient pressure matches with experimentally measured subharmonic response as a function of ambient pressure, while assuming constant material parameters does not.

© 2015 Acoustical Society of America. [<http://dx.doi.org/10.1121/1.4923364>]

[CCC]

Pages: 624–634

## I. INTRODUCTION

Gas-filled microbubbles (diameter  $<10 \mu\text{m}$ ) coated with lipids, proteins, polymers, and other surface active materials are an excellent agent for enhancing the contrast of medical ultrasound images (Goldberg *et al.*, 2001; Nahire *et al.*, 2013; Nahire *et al.*, 2014; Paul *et al.*, 2014). The coating stabilizes the microbubbles against premature dissolution (Katiyar *et al.*, 2009; Sarkar *et al.*, 2009), but it also significantly changes their mechanical properties and therefore the echogenicity. Many models of these ultrasound contrast agents (UCA) have been developed and applied to different agents to determine the mechanical properties of their encapsulation (deJong *et al.*, 1992; deJong *et al.*, 1994; Church, 1995; Chatterjee and Sarkar, 2003; Marmottant *et al.*, 2005; Sarkar *et al.*, 2005; Paul *et al.*, 2010; Paul *et al.*, 2014). Although they are Food and Drug Administration approved only for cardiovascular imaging in the United States, active investigations are underway for their use in other organs such as liver, kidney, and brain. The blood pressure varies widely between these organs which can drastically affect the ultrasound response of the UCAs. Here, we investigate the effects of ambient hydrostatic pressure variation on the material properties of the encapsulation of a contrast agent using ultrasound attenuation data obtained under varying ambient pressure.

As we noted above there have been many models of the encapsulation of UCAs starting since the early 1990s with adoption of effective shell elasticity  $S_p$  and friction  $S_f$

factors in Rayleigh-Plesset equation (deJong *et al.*, 1992). Church offered the first rigorous constitutive model assuming the encapsulation to be a layer of linear viscoelastic material (Church, 1995). However, the encapsulating layer being at most a-few-molecule thick, we argued in 2003 that it should be modeled as a zero-thickness interface with its intrinsic interfacial rheology (Chatterjee and Sarkar, 2003). Over the years we have developed Newtonian (NM), constant viscous-elastic (CEM) and strain-softening nonlinear exponential elastic (EEM) models and applied to a number of different contrast agents to measure their interfacial rheology (Sarkar *et al.*, 2005; Paul *et al.*, 2010; Paul *et al.*, 2013). There have been other models—very similar to the CEM and the EEM model but allowing for shell rupture and buckling (Marmottant *et al.*, 2005), hyperelastic membrane model (Tsigliffis and Pelekasis, 2008) and nonlinear viscous model (Doynikov and Dayton, 2007) to describe the contrast agent dynamics. Recently, we have shown that a general interfacial rheological form can represent a number of different models with an effective surface tension and a surface dilatational elasticity (Katiyar and Sarkar, 2011).

Contrast agent dynamics is also affected by the surrounding environment—temperature, pressure and the acoustic excitation. Recently, investigations have been performed to characterize how their properties vary with bubble size, temperature and excitation frequency (Goertz *et al.*, 2007). We have investigated the effects of ambient pressure variation on subharmonic emissions from contrast agents (Katiyar *et al.*, 2011). However, the study assumed that the material properties remain unchanged with the varying pressure.

<sup>a)</sup>Electronic mail: [sarkar@gwu.edu](mailto:sarkar@gwu.edu)

Contrast agents experience widely different pressures in different organs. The typical blood pressure in portal vein (D'amico *et al.*, 1995), pulmonary artery (Simonneau *et al.*, 2009), and left ventricle (systolic) (Lawes *et al.*, 2004) are 5–10 mm Hg, 8–20 mm Hg, and 100–140 mm Hg, respectively. Therefore, it is important to assess whether the acoustic response/encapsulation properties are influenced by ambient pressure. Furthermore, ambient pressure in an organ may also vary because of a disease as in portal hypertension. Recently, there has been an effort to noninvasively estimate organ level pressure using contrast enhanced ultrasound (Bouakaz *et al.*, 1999; Shi *et al.*, 1999a,b; Shi *et al.*, 2002; Adam *et al.*, 2005; Leodore *et al.*, 2007; Andersen and Jensen, 2010; Halldorsdottir *et al.*, 2011) for disease diagnosis. Forsberg *et al.* have proposed and patented subharmonic aided pressure estimation (SHAPE). They have recently shown through *in vitro* experiments with a number of contrast agents that subharmonic response decreases by 9 to 14 dB when the hydrostatic pressure was increased from 0 to 186 mm Hg (Halldorsdottir *et al.*, 2011). However, Frinking *et al.* (2010) found that the subharmonic response from a phospholipid coated bubble (Sonovue from Bracco, Milano, Italy) increased by 28.9 dB for 180 mm Hg increase of ambient pressure with a relatively low acoustic excitation of 50 kPa. We have recently shown theoretically that subharmonic response from a bubble can both decrease or increase with ambient pressure increase depending on the ratio of the excitation frequency to its natural frequency (Katiyar *et al.*, 2011).

The objective of the present work is to investigate whether and how the encapsulation of a UCA changes with change in ambient pressure. We use previously developed interfacial models to contrast agents to determine their properties. Phospholipid shelled UCA—Definity<sup>®</sup> (Lantheus Imaging, North Billerica, MA) is the subject of this study. Definity has been investigated before (Chatterjee *et al.*, 2005b; Goertz *et al.*, 2007; Faez *et al.*, 2011; Helfield *et al.*, 2012), but their mechanical properties as functions of ambient pressure has not been measured. We use ultrasound attenuation through contrast agents for the parameter estimation. In Sec. II, we provide the mathematical models as well as the experimental procedure for our investigation. Section III describes the result, and Sec. IV offers concluding remarks.

## II. PROCEDURE FOR ESTIMATING THE ENCAPSULATION PARAMETERS

In our earlier publications (Chatterjee and Sarkar, 2003; Sarkar *et al.*, 2005; Paul *et al.*, 2010; Paul *et al.*, 2013), we have developed a detailed procedure for characterizing the mechanical properties of a contrast agent using experimentally measured ultrasound attenuation through contrast agent suspension. Here, we provide only a brief sketch of the methodology.

### A. Mathematical models

The contrast microbubble dynamics is described by a modified Rayleigh-Plesset equation with various

encapsulation models. We have recently shown that many different encapsulation models, including those with a finite thickness such as the one by Church (1995) in the limit of small thickness, can be written as a general Rayleigh-Plesset equation with effective interfacial properties—effective surface tension  $\gamma(R)$  and interfacial dilatational viscosity  $\kappa^s(R)$  (Paul *et al.*, 2010). It describes the radial motion  $R(t)$ ,

$$\rho \left( R\ddot{R} + \frac{3}{2}\dot{R}^2 \right) = P_g \left( 1 - 3\kappa \frac{\dot{R}}{c} \right) - 4\mu \frac{\dot{R}}{R} - \frac{4\kappa_s(R)\dot{R}}{R^2} - \frac{2\gamma(R)}{R} - P_0 + P_A \sin \omega t. \quad (1)$$

Here,  $\rho$  is the density of the liquid,  $P_g$  is the gas pressure inside the bubble which expands with a polytropic coefficient  $\kappa$ ,  $c$  is the speed of sound in the liquid,  $\mu$  is its viscosity, and  $P_0$  is the ambient pressure. Since with oscillations at MHz frequency Peclet number  $Pe = R_0^2 \omega / D_g \gg 1$  ( $D_g$  is the thermal diffusivity; for  $C_3F_8$   $2.8 \times 10^{-6}$  m<sup>2</sup>/s), we assume an adiabatic behavior for the gas inside ( $\kappa = \kappa_{ad} = 1.07$  for  $C_3F_8$  and 1.4 for air). The bubble is responding to an ultrasound wave with amplitude  $P_A$  and circular frequency  $\omega$ . We use four different encapsulation models.

#### 1. Newtonian model (NM)

$$\gamma(R) = \gamma(\text{constant}) \quad \text{and} \quad \kappa^s(R) = \kappa^s(\text{constant}), \quad (2)$$

$$f_0 = \frac{1}{2\pi R_0} \sqrt{\frac{1}{\rho} \left( 3\kappa P_0 + \frac{2\gamma}{R_0} (3\kappa - 1) \right)}. \quad (3)$$

#### 2. Constant elasticity viscoelastic model (CEM)

$$\gamma(R) = \gamma_0 + E^s \beta, \quad \beta = \left( \frac{\Delta \text{Area}}{\text{Area}_{\text{equilibrium}}} \right) = \left( \frac{R^2}{R_E^2} - 1 \right) \quad \text{and} \quad \kappa^s(R) = \kappa^s(\text{constant}), \quad (4)$$

where  $\gamma_0$  is a constant, a reference value of the interfacial tension and  $E^s$  is the constant dilatational elasticity. Note that the restriction of  $\gamma(R) > 0$  has been relaxed here in contrast to some of our earlier publications. In fact, non-negative surface tension was found to lead to neutral stability against dissolution by gas diffusion (Katiyar and Sarkar, 2010). The equilibrium radius  $R_E$  is given by  $R_E = R_0(1 - \gamma_0/E^s)^{-1/2}$ . This ensures a balance of inside and outside pressure at initial radius. At the equilibrium radius the bubble encapsulation has no elastic stresses,

$$f_0 = \frac{1}{2\pi R_0} \sqrt{\frac{1}{\rho} \left( 3\kappa P_0 - \frac{4\gamma_0}{R_0} + \frac{4E^s}{R_0} \right)}. \quad (5)$$

For model A2 for gas diffusion in Sec. IID below, we assume  $R_E = R_0$ . Then one obtains

$$f_0 = \frac{1}{2\pi R_0} \sqrt{\frac{1}{\rho} \left( 3\kappa P_0 + \frac{2\gamma_0}{R_0} (3\kappa - 1) + \frac{4E^s}{R_0} \right)}. \quad (6)$$

### 3. Viscoelastic model with exponentially varying elasticity (EEM)

$$\begin{aligned} \gamma(R) &= \gamma_0 + E^s \beta \quad \text{and} \quad \kappa^s(R) = \kappa^s(\text{constant}), \\ E^s &= E_0^s \exp(-\alpha^s \beta). \end{aligned} \quad (7)$$

Enforcing balance of pressure at initial radius, we obtain

$$R_E = R_0 \left[ 1 + \left( \frac{1 - \sqrt{1 + 4\gamma_0 \alpha^s / E_0^s}}{2\alpha} \right)^{-1/2} \right], \quad (8)$$

$$f_0 = \frac{1}{2\pi R_0} \sqrt{\frac{1}{\rho} \left( 3\kappa P_0 + \frac{2E_0^s}{R_0} \left( \frac{\sqrt{1 + 4\gamma_0 \alpha^s / E_0^s}}{\alpha^s} \right) \left( 1 + 2\alpha^s - \sqrt{1 + 4\gamma_0 \alpha^s / E_0^s} \right) \right)}. \quad (9)$$

For  $R_E = R_0$  (model A2 of gas diffusion in Sec. II D) one obtains resonance frequency same as in Eq. (6).

### 4. Marmottant model (MM)

$$\gamma(R) = \begin{cases} 0 & \text{for } R \leq R_{\text{buckling}} \\ \chi \left( \frac{R^2}{R_{\text{buckling}}^2} - 1 \right) & \text{for } R_{\text{buckling}} \leq R \leq R_{\text{rupture}} \text{ and } \kappa^s(R) = \kappa^s(\text{constant}) \\ \gamma_w & \text{for } R \geq R_{\text{rupture}}, \end{cases} \quad (10)$$

where  $\chi$  [same as  $E^s$  in Eq. (4)] is the elastic modulus of the shell,  $R_{\text{buckling}} = R_0 [1 + \gamma(R_0)/\chi]^{-1/2}$  and  $R_{\text{rupture}} = R_{\text{buckling}} [1 + \gamma_w/\chi]^{1/2}$ . Above  $R_{\text{rupture}}$ , the bubble is assumed to have a pure air-water interface and below  $R_{\text{buckling}}$ , it is in a buckled state where the effective interfacial tension is zero,

$$f_0 = \frac{1}{2\pi R_0} \sqrt{\frac{1}{\rho} \left( 3\kappa P_0 - \frac{2\gamma(R_0)}{R_0} (3\kappa - 1) + \frac{4\chi}{R_0} \right)}. \quad (11)$$

### B. Ultrasound attenuation and estimation of interfacial rheological parameters

We measure attenuation of ultrasound through a contrast agent suspension at a sufficiently low excitation to ensure a linear behavior of the contrast microbubbles (Chatterjee *et al.*, 2005b). In this regime, the linearized Rayleigh-Plesset equation leads to a simple harmonic motion characterized by an undamped resonance frequency  $f_0 = \omega_0/2\pi$  and a nondimensional damping term  $\delta$  (Paul *et al.*, 2010; Paul *et al.*, 2013). The damping is caused by four different mechanisms: liquid viscosity, encapsulation, acoustic radiation, and thermal (Hoff *et al.*, 2000),

$$\begin{aligned} \delta &= \delta_{\text{liquid}} + \delta_{\text{encapsulation}} + \delta_{\text{radiation}} + \delta_{\text{thermal}} \\ &= \frac{4\mu}{\rho\omega_0 R_0^2} + \frac{4\kappa^s}{\rho\omega_0 R_0^3} + \frac{3\kappa P_0}{\rho\omega_0 R_0 c} \\ &\quad + \frac{1}{\omega\omega_0} \frac{3P_0}{\rho R_0^2} \text{Im} \left( \frac{1}{\Phi(R_0, \omega)} \right), \\ \Phi(R_0, \omega) &= \frac{1}{\kappa_{ad}} \left( 1 + \frac{3(\kappa_{ad} - 1)}{X^2} (X \coth X - 1) \right), \\ X(R_0, \omega) &= R_0 \sqrt{\frac{i\omega}{D_g}}. \end{aligned} \quad (12)$$

Here  $D_g$  is the thermal diffusivity (for  $\text{C}_3\text{F}_8$   $2.8 \times 10^{-6}$  m<sup>2</sup>/s) and  $\kappa_{ad}$  is the adiabatic constant equal to the ratio of specific heats. The encapsulation damping is by far the largest component of the four damping terms for contrast microbubbles (Katiyar and Sarkar, 2012). The extinction cross-section  $\sigma_e$  for the linearized dynamics can be computed as (Sarkar and Prosperetti, 1994; Sarkar *et al.*, 2005)

$$\sigma_e = 4\pi R_0^2 \frac{c\delta}{\omega_0 R_0} \frac{\Omega^2}{[(1 - \Omega^2)^2 + \Omega^2 \delta^2]}, \quad \Omega = \frac{\omega_0}{\omega}, \quad (13)$$

giving rise to attenuation  $\theta(\omega)$  in dB/distance

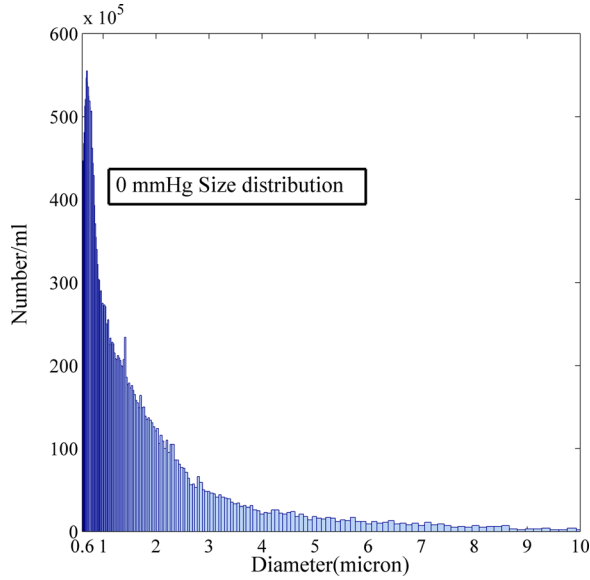


FIG. 1. (Color online) Size distribution of Definity microbubble.

$$\theta(\omega) = 10 \log_{10} e \int_{R_{\min}}^{R_{\max}} \sigma_e(R; \omega) n(R) dR, \quad (14)$$

where  $e$  is the base of natural logarithm,  $n(R)dR$  is the number of bubbles per unit volume with radius in the range  $(R, R + dR)$ , and the range of bubble radii is given by  $(R_{\min}, R_{\max})$ . By measuring the size distribution, we can derive a theoretical expression of attenuation using the different models. An error function between the measured and the modeled attenuation is minimized to find the interfacial rheological parameters, e.g.,  $\gamma$ ,  $\kappa^s$ ,  $E^s$ ,  $\alpha^s$ , etc.

### C. Contrast agents and their size distribution

We investigate Definity microbubbles in this work. Figure 1 shows size distribution of Definity microbubbles at 0 mm Hg of overpressure, i.e., at 1 atmosphere (atm) pressure. The size distribution of Definity microbubble is obtained using Coulter Counter in the lab of Professor Christy Holland and has been previously reported in the literature (Raymond *et al.*, 2014). Definity microbubble has an average diameter  $1.2 \mu\text{m}$ . Note that the very small size particles might not be registered by the instrument. However, their scattering and attenuation cross-sections also are small to have a significant effect on the attenuation spectra. The size distribution is similar to the one obtained previously by others (Faez *et al.*, 2011).

### D. Size change due to overpressure

Overpressure change can affect the size of a contrast microbubble by mechanical compression as well as by gas transfer through the encapsulation. The latter process depends on the permeability of the encapsulating layer. It is well known that contrast agents such as Definity that are stored in vials with the headspace filled with the perfluorocarbon (PFC) gas, when dissolved in water or a buffer solution, experiences an initial swelling due to gas exchange. The ingress of air from outside far outweighs the outward diffusion of PFC due to latter's poor solubility and smaller diffusivity. In the long run, air

completely replaces PFC leaving an air-filled microbubble. Therefore, gas exchange plays an important role in determining the size of the contrast microbubbles and thereby their acoustic properties (Chatterjee *et al.*, 2005a; Chatterjee *et al.*, 2005b). We have mathematically modeled diffusion of PFC and air through the encapsulation layer (Epstein and Plesset, 1950; Borden and Longo, 2002; Katiyar *et al.*, 2009; Sarkar *et al.*, 2009). Here, we only briefly mention the underlying physics. Gases diffuse in the surrounding medium down their concentration gradients. While the gas concentration far away from the bubble is determined by the bulk saturation level of the medium, near the interface the surrounding liquid is considered to be at equilibrium with the gas inside the bubble (Henry's law). The surface tension at the interface makes the pressure inside the bubble higher by an amount equal to the Laplace pressure. The gas diffusion from or into the microbubbles is driven by the effective surface tension and the gas saturation level of the surrounding medium. Mathematical models have been able to describe the initial increase in bubble radius and later dissolution and final equilibrium radius (Sarkar *et al.*, 2009). Note that when PFC diffusion, however small, is taken into account, the final microbubble becomes an air-filled one (Sarkar *et al.*, 2005; Paul *et al.*, 2010).

Sudden increase of overpressure leads to a transient disequilibrium which can give rise to gas diffusion process from/into the microbubble. It is reasonable to assume that even upon the increase of overpressure, the liquid far away remains at the saturation level consistent with the atmospheric pressure  $p_{\text{atm}}$ , whereas the dissolved gas concentration immediately adjacent to the bubble changes to a new value. Such a disequilibrium is at the heart of the air expulsion and size decrease under overpressure increase. There are many parameters that governs the process, and currently there are considerable uncertainties in their values. We, therefore, consider three different approaches/approximations to model the radius change due to gas diffusion under overpressure increase: model A1, without any mass exchange the radius changes by mechanical compression; model A2, due to the low diffusivity and solubility, PFC content remains unchanged, and only air diffuses out of an air-PFC-microbubble under increased pressure; and model A3, sufficient time has passed for the bubble be an air-filled one, where again air diffuses out under increasing overpressure.

#### 1. Model A1: No gas exchange

With initial condition of  $\dot{R} = \ddot{R} = 0$ , Eq. (1) reduces to

$$P_{g0} = \frac{2\gamma(R_0)}{R_0} + P_0, \quad P_0 = p_{\text{atm}} + p_{\text{over}}. \quad (15)$$

$P_{g0}$  is the initial gas pressure inside the bubble with the initial radius  $R_0$ . At ambient pressure (overpressure  $p_{\text{over}} = 0$ ), one obtains the initial gas pressure as  $P_{g0}^0 = p_{\text{atm}}$ , where the surface tension for zero ambient overpressure  $\gamma(R_0^0)$  is assumed to be zero at initial radius  $R_0^0$ ; it ensures microbubble stability against gas diffusion. Assuming an adiabatic process for the gas inside the bubble, the initial bubble radius would change from  $R_0^0$  to  $R_0$  when subjected to nonzero overpressure according to

$$\frac{2}{R_0} \left( \gamma_0 + E^s \left( \left( \frac{R_0}{R_E} \right)^2 - 1 \right) \right) + p_{\text{atm}} + p_{\text{over}} = p_{\text{atm}} \left( \frac{R_0^0}{R_0} \right)^{3k}. \quad (16)$$

To solve this equation at nonzero  $p_{\text{over}}$ ,  $\gamma(R_0)$  is expressed as in Eq. (4) using values of  $\gamma_0$  and  $E^s$  obtained at zero overpressure as an approximation. This approximation is used in all three approaches. After interfacial rheological properties are estimated at nonzero overpressure, they are then used to iteratively improve this approximation to find little difference in result.

## 2. Model A2: Bubble retains PFC and air diffuses out

Initially bubble is filled with PFC, and the PFC content is assumed to remain unchanged through the process because of its low permeability through the membrane as well as low diffusivity and solubility in the liquid. At any instant the net gas pressure inside the microbubble, comprising now of air and PFC at partial pressures  $p_A$  and  $p_F$ , is again described by (15),

$$p_A + p_F = \frac{2\gamma(R)}{R_0} + p_{\text{atm}} + p_{\text{over}}. \quad (17)$$

We assume that at each overpressure level, air pressure reaches an equilibrium with the outside medium. The surrounding medium far away is assumed to be saturated with air at atmospheric pressure  $p_{\text{atm}}$  even though the ambient pressure is increased. Therefore, as per Henry's law, dissolved air concentration far away from bubble  $C_A(\infty)$  and in the liquid adjacent to the microbubble, containing air at pressure  $p_A$ ,  $C_A(R)$  are

$$C_A(\infty) = L_A \frac{p_{\text{atm}}}{R_G T}, \quad C_A(R) = L_A \frac{p_A}{R_G T}. \quad (18)$$

$L_A$  is the Ostwald coefficient relating dissolved concentration to adjacent gas concentration.  $R_G$  and  $T$  are the universal gas constant and the temperature, respectively. After overpressure change gas exchange and accompanying diffusion leads to an equilibrium  $C_A(\infty) = C_A(R)$  (i.e., no further diffusion) obtaining

$$p_A = p_{\text{atm}}. \quad (19)$$

At zero overpressure therefore, Eq. (17) gives rise to

$$p_F = \frac{n_F R_G T}{\frac{4}{3} \pi (R_0^0)^3} = \frac{2\gamma(R_0^0)}{R_0^0} = \frac{2\gamma_0}{R_0^0}. \quad (20)$$

The number of moles  $n_F$  of PFC remains constant even with pressure change, as PFC does not diffuse in/out of the bubble. Note that with this consideration, one cannot assume  $\gamma(R_0^0) = 0$ . Instead, here we assume  $R_E = R_0^0$ , i.e., at ambient pressure the encapsulation is at a stress-free condition, which leads to the second equality in Eq. (20). At nonzero overpressure one obtains

$$p_F = \frac{n_F R_G T}{\frac{4}{3} \pi (R_0)^3} = \frac{2\gamma(R_0)}{R_0} + p_{\text{over}} \quad \text{or} \quad \frac{2\gamma_0}{R_0^0} \left( \frac{R_0^0}{R_0} \right)^3 = \frac{2}{R_0} \left( \gamma_0 + E^s \left( \left( \frac{R_0}{R_0^0} \right)^2 - 1 \right) \right) + p_{\text{over}}. \quad (21)$$

Solving it one obtains  $R_0$  at new overpressure  $p_{\text{over}}$ .

## 3. Model A3: Air-filled bubble exchanging air with medium

If both PFC and air are allowed to diffuse through the encapsulation, eventually all PFC would diffuse out into the surrounding medium leaving air-filled microbubbles. Again, the same consideration as in model A2 gives rise to air pressure equilibrium (19). At  $p_{\text{over}} = 0$ , assuming a steady bubble warrants  $\gamma(R_0^0) = 0$ . At other overpressures

$$\frac{2\gamma(R_0)}{R_0} + p_{\text{over}} = 0 \quad \text{or} \quad \frac{2}{R_0} \left( \gamma_0 + E^s \left( \left( \frac{R_0}{R_E} \right)^2 - 1 \right) \right) + p_{\text{over}} = 0, \quad (22)$$

which is solved for obtaining  $R_0$ .

The bubble radius decreases under overpressure increase for all three different models. Figure 2 shows the predicted percentage decrease in radius with overpressure using each of the above-mentioned models. The model that considers no gas diffusion (A1) predictably results in the least amount of decrease in radius. The other two models (A2 and A3) gives rise to very similar results. Below, while determining the rheological properties, we use all three models to determine the changed radius distribution under overpressure change.

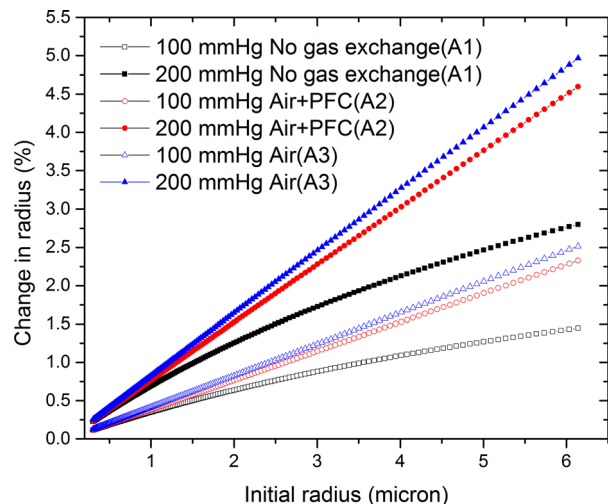


FIG. 2. (Color online) Percentage change in radius over its value at the atmospheric pressure at two different ambient overpressure according to three different models A1, A2, and A3 of bubble size change.

## E. Effects of ambient pressure on number of microbubbles

Definity microbubbles are considered fairly stable to pressure change experienced inside the body. We here check the possibility of microbubble destruction and thereby decrease in the number of microbubbles under overpressure. We measure attenuation in a fresh solution of microbubbles at atmospheric pressure. Then, we subject it to an overpressure for 2.5 min and then release the overpressure to bring the pressure back to the atmospheric pressure. Attenuation is measured again to find very similar values in two cases for most of the frequencies. The results are obtained for two different overpressure values (Fig. 3), and experiments are repeated five times for each overpressure value. On the basis of this experiment, it is reasonable to assume that there is little to no destruction of microbubbles because of pressure change. Note that Hoff investigated attenuation before and after subjecting the contrast agent to an overpressure of 120 mm Hg for 30 s to find them reasonably similar (Hoff, 2001).

## F. Experimental setup and procedure to measure attenuation

Figure 4(a) shows a schematic of the experimental setup. An airtight chamber (50 mm × 50 mm × 45 mm) made of polycarbonate was filled with the contrast agent suspension [Fig. 4(b)]. Attenuation from a suspension of contrast agent (constantly stirred) was measured using an unfocused broadband transducer (Olympus NDT, Waltham, MA) with a central frequency of 3.5 MHz operated in transmit/receive mode. The -6 dB bandwidth of the transducer was 2.5 to 4.99 MHz. A pulser/receiver (model 5800; Panametrics-NDT, Waltham, MA) was used to excite the transducers with a broadband pulse of PRF of 100 Hz with peak amplitude of 35 kPa at 3.5 MHz. The pulse generated by the transducer traveled a total distance of 10 cm through the contrast agent suspension (from the transducer face to the chamber wall and back)

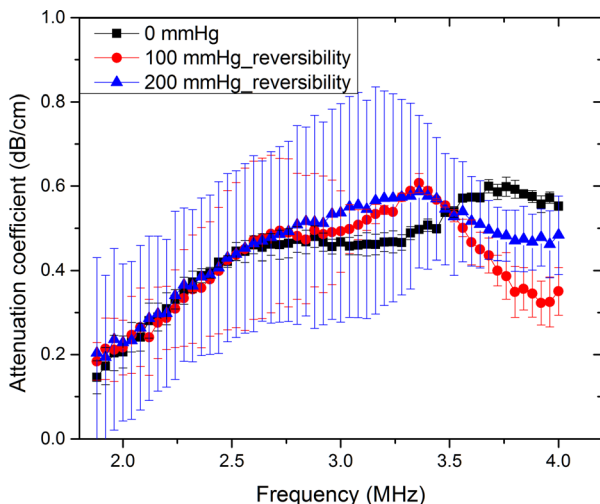


FIG. 3. (Color online) Pressure reversibility: Attenuation at ambient pressures before (0 mm Hg) and after they were subjected to overpressures (100 and 200 mm Hg) for 2.5 min.

before being received and fed to the digital oscilloscope (Model TDS 2012; Tektronix, Beaverton, OR) to observe the signal in real time. A pressure gauge (SSI Technologies, Janesville, WI) was used to measure the static pressure of the chamber. Signals were acquired from the oscilloscope using LabView (National Instruments, Austin, TX) software. Fifty voltage-time RF traces were acquired in an averaging mode (64 sequences are used for averaging) and saved.

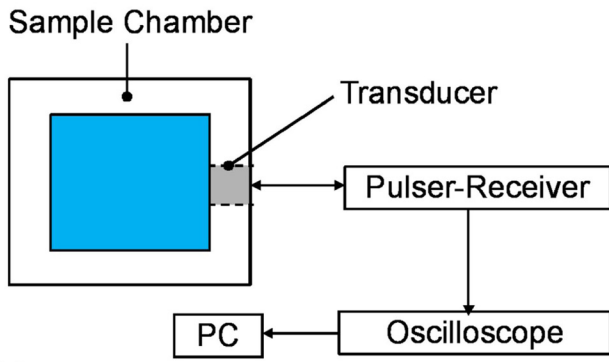
Definity microbubbles were used for the experiment. Definity microbubble was reconstituted from its vial following the established protocol using vialmixer for 45 s. The 10  $\mu$ l of microbubble solution was drawn from the vial, using a microliter syringe, 1 minute after activation and dissolved in 100 ml of PBS buffer solution. Each attenuation experiment was repeated five times, i.e., five data sets were collected from five new suspensions prepared from the vial solution. This sequence of experiments was repeated at each overpressure. For attenuation measurement, signals were obtained with and without UCAs. The voltage time response acquired was converted to frequency domain using fast Fourier transform (FFT). The power spectrum was averaged for 50 acquisitions. The frequency dependent attenuation coefficient was calculated using the following expression

$$\alpha(\omega) = 20 \log_{10} \left( \frac{\bar{V}_{\text{ref}}(\omega)}{\bar{V}_{\text{sig}}(\omega)} \right) / d, \quad (23)$$

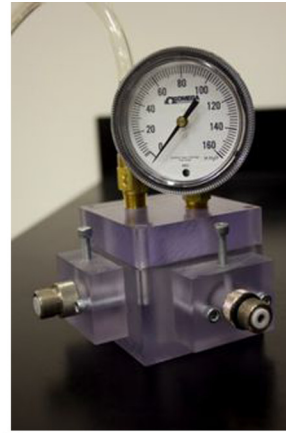
where  $\bar{V}_{\text{ref}}(\omega)$  is the averaged response in the frequency domain without any contrast agent in the medium,  $\bar{V}_{\text{sig}}(\omega)$  is the averaged response in the frequency domain microbubbles suspended in the medium, and  $d = 10$  cm is the total path traveled by the pulse before it is being received by the transducer. Note that multiple scattering has been neglected as is the common practice; individual microbubbles are separated by hundreds of wavelengths.

## G. Experimental setup and procedure to measure scattering and comparison with model

Figure 5 shows a schematic of the experimental setup to measure scattering from contrast agent suspension under different ambient pressures. The air-tight chamber used for measuring attenuation [Fig. 2(b)] is also used here. The experimental setup employed two spherically focused immersion transducers (Panametrics Transducer, Olympus NDT Corporation, Waltham, MA), each having an individual diameter of 1.6 cm and a focal length of 3.05 cm. The transmitting and receiving transducers were confocally positioned at right angles. 100 ml of bubble suspension is taken in the chamber. An arbitrary/function generator (Model AFG 3251; Tektronix, Beaverton, OR) was utilized to generate a 32 cycle sinusoidal pulse of desired frequency at a PRF of 100 Hz. This signal was then amplified using a 55 dB power amplifier (model A-150, ENI, Rochester, NY) and fed to the transmitting transducer. The scattered signal was received by the receiving transducer utilizing a pulser/receiver in receiving mode with a 20 dB gain. The amplified signals were then fed to the oscilloscope to view them in real time. Ambient pressure inside the chamber was measured using a pressure



(a)



(b)

FIG. 4. (Color online) (a) Schematic of the experimental setup to measure acoustic attenuation. (b) Airtight chamber.

gauge (OMEGA Engineering, Stamford, CT). Measurement for each setting was repeated 5 times and each time fresh bubble suspension was used. Experimentally measured scattering was compared with the model prediction at different ambient pressure. The model prediction was computed using the far field pressure  $P_S(r, t)$  scattered by the microbubbles (Brennen, 1995)

$$P_S(r, t) = \rho \frac{R}{r} (2\dot{R}^2 + R\ddot{R}) \quad \text{and} \quad \sigma_s(r, t) = \frac{4\pi \langle r^2 P_S(r, t)^2 \rangle}{P_A^2}. \quad (24)$$

$\sigma_s(r, t)$  is the scattering cross-section. Computed scattered power is transformed into frequency domain by FFT and the total scattered power is computed integrating contributions from bubbles of all radii from  $R_{\min}$  to  $R_{\max}$ ,

$$S_s(\omega) = \int_{R_{\min}}^{R_{\max}} \sigma_s(R; \omega) n(R) dR. \quad (25)$$

Here  $n$  is the number of microbubbles per unit volume per unit radius. The subharmonic response is extracted from the power spectrum and compared with experimental result.

### III. RESULTS AND DISCUSSION

Figure 6 plots the measured attenuation curves at three different overpressures for Definity microbubbles. The attenuation decreases with the increase of ambient overpressure. Any of the relations for resonance frequency, e.g., Eqs.

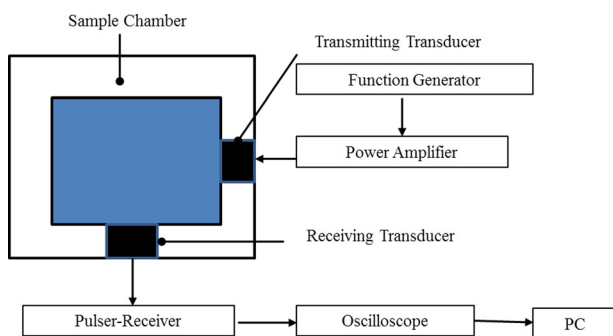


FIG. 5. (Color online) Schematic of the experimental setup to measure acoustic scattering.

(3) or (5), shows that the resonance frequency for a microbubble with a given radius increases with an increase in ambient overpressure provided other properties remain unchanged. For a mono-dispersed suspension of microbubbles the peak of the attenuation curve occurs at the resonance frequency. For a poly-dispersed suspension, the peak represents a weighted average resonance frequency of the suspension. The peak of the attenuation curve here shifts toward right—higher frequencies—with increase of ambient overpressure, i.e., the weighted average resonance frequency increases. The encapsulation parameters are estimated by the method mentioned in Sec. II. Figure 6 shows the model attenuation curves according to EEM model fitted to the experimental measurement [corresponding root-mean-square error values in the minimization are 0.0837 (0 mm Hg), 0.2173 (100 mm Hg) and 0.0452 (200 mm Hg)]. Table I present the values of encapsulation parameters for Definity microbubbles for various encapsulation models.

Because of the similarity between the models in the linear range the properties estimated by different models are very similar; more complex interfacial models, of course, have more parameters. The parameters are obtained using model A2 of gas diffusion that assumes that PFC content of a microbubble remains constant and only air diffuses out

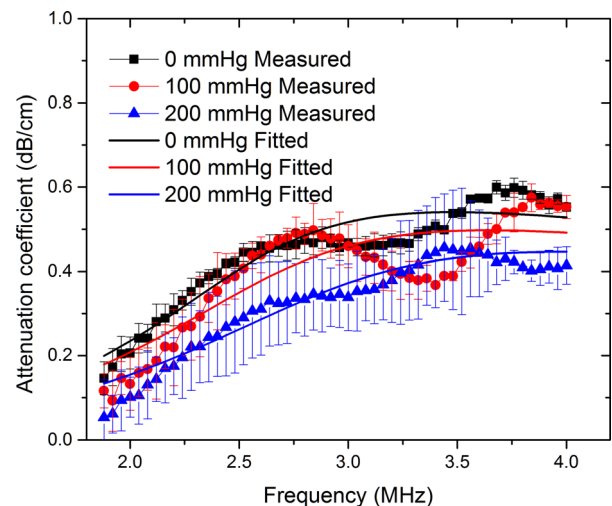


FIG. 6. (Color online) Measured frequency dependent attenuation curves at different ambient overpressures along with EEM model predictions.

TABLE I. Estimated property values of Definity microbubbles.

Encapsulation Model	Encapsulation parameters	0 mm Hg	100 mm Hg	200 mm Hg
NM	$\kappa^s (\times 10^{-8} \text{N s/m})$	$3.43 \pm 0.07$	$3.82 \pm 0.06$	$4.21 \pm 0.05$
	$\gamma (\text{N/m})$	$0.797 \pm 0.01$	$0.827 \pm 0.01$	$0.992 \pm 0.01$
CEM	$\kappa^s (\times 10^{-8} \text{N s/m})$	$3.61 \pm 0.06$	$4.0 \pm 0.05$	$4.43 \pm 0.08$
	$\gamma_0 (\text{N/m})$	$0.01 \pm 0.01$	$0.01 \pm 0.01$	$0.01 \pm 0.01$
	$E^s (\text{N/m})$	$0.86 \pm 0.01$	$0.894 \pm 0.01$	$1.07 \pm 0.02$
EEM	$\kappa^s (\times 10^{-8} \text{N s/m})$	$3.6 \pm 0.03$	$3.99 \pm 0.03$	$4.4 \pm 0.06$
	$E_0^s (\text{N/m})$	$0.86 \pm 0.01$	$0.894 \pm 0.01$	$1.06 \pm 0.02$
	$\alpha$	$1 \pm 0.2$	$1 \pm 0.7$	$1 \pm 0.2$
	$\gamma_0 (\text{N/m})$	$0.01 \pm 0.004$	$0.01 \pm 0.01$	$0.01 \pm 0.01$
MM	$\kappa^s (\times 10^{-8} \text{N s/m})$	$3.66 \pm 0.04$	$4.05 \pm 0.04$	$4.48 \pm 0.06$
	$\chi (\text{N/m})$	$0.867 \pm 0.01$	$0.89 \pm 0.02$	$1.09 \pm 0.02$

TABLE II. Property values of Definity microbubbles using different approaches for calculating initial radius at various overpressure.

Approach of calculating initial radius at overpressure	Encapsulation parameters	0 mm Hg	100 mm Hg	200 mm Hg
No gas exchange (A1)	$\kappa^s (\times 10^{-8} \text{N s/m})$	$3.6 \pm 0.03$	$4.01 \pm 0.03$	$4.34 \pm 0.06$
	$E_0^s (\text{N/m})$	$0.86 \pm 0.01$	$0.898 \pm 0.01$	$1.09 \pm 0.02$
	$\alpha$	$1 \pm 0.2$	$1 \pm 0.5$	$1 \pm 0.2$
	$\gamma_0 (\text{N/m})$	$0.01 \pm 0.004$	$0.01 \pm 0.01$	$0.01 \pm 0.01$
Bubble retains PFC and air diffuses (A2)	$\kappa^s (\times 10^{-8} \text{N s/m})$	$3.6 \pm 0.03$	$3.99 \pm 0.03$	$4.4 \pm 0.06$
	$E_0^s (\text{N/m})$	$0.86 \pm 0.01$	$0.894 \pm 0.01$	$1.06 \pm 0.02$
	$\alpha$	$1 \pm 0.2$	$1 \pm 0.7$	$1 \pm 0.2$
	$\gamma_0 (\text{N/m})$	$0.01 \pm 0.004$	$0.01 \pm 0.01$	$0.01 \pm 0.01$
Air-filled bubble exchanging air with medium (A3)	$\kappa^s (\times 10^{-8} \text{N s/m})$	$3.66 \pm 0.03$	$4.05 \pm 0.03$	$4.45 \pm 0.06$
	$E_0^s (\text{N/m})$	$0.81 \pm 0.01$	$0.84 \pm 0.01$	$1.0 \pm 0.02$
	$\alpha$	$1 \pm 0.2$	$1 \pm 0.7$	$1 \pm 0.2$
	$\gamma_0 (\text{N/m})$	$0.01 \pm 0.004$	$0.01 \pm 0.01$	$0.01 \pm 0.01$
No change in size	$\kappa^s (\times 10^{-8} \text{N s/m})$	$3.6 \pm 0.03$	$4.1 \pm 0.03$	$4.65 \pm 0.06$
	$E_0^s (\text{N/m})$	$0.86 \pm 0.01$	$0.895 \pm 0.01$	$1.12 \pm 0.02$
	$\alpha$	$1 \pm 0.2$	$2 \pm 0.7$	$1 \pm 0.2$
	$\gamma_0 (\text{N/m})$	$0.01 \pm 0.004$	$0.01 \pm 0.01$	$0.01 \pm 0.01$

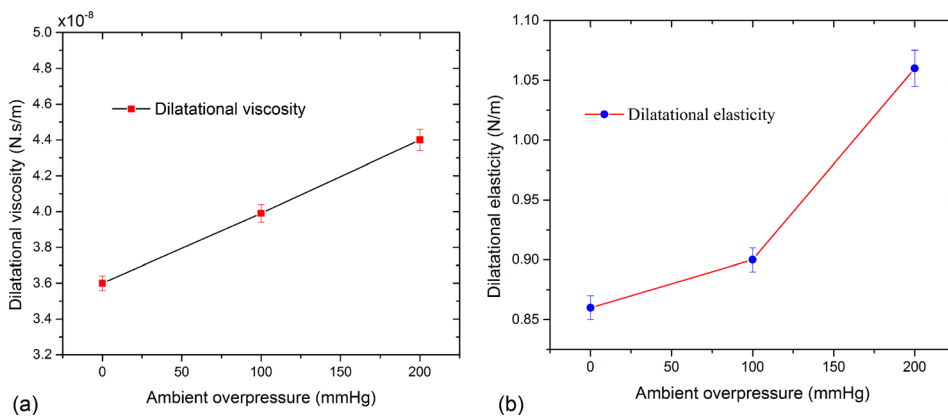


FIG. 7. (Color online) Variation in (a) dilatational viscosity and (b) dilatational elasticity with change in ambient pressure according to EEM model.

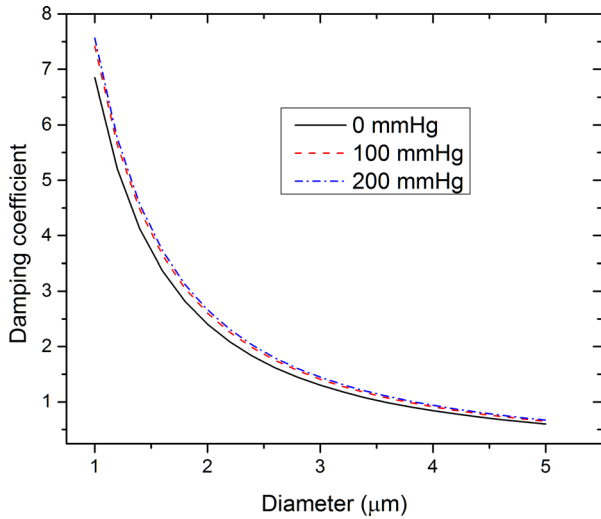


FIG. 8. (Color online) Damping coefficient  $\delta$  as a function of diameter at different ambient pressures (EEM model).

under overpressure reducing the bubble size. In Table II, we list EEM rheological properties according to A1 (no gas exchange) and A3 (air filled bubble exchanging air) models of gas diffusion also. Each model has new bubble size under overpressures. The rheological properties determined under different diffusion models are similar. For the rest of the article, we show results only for the EEM model along with the A2 model of gas diffusion.

Also note that the rheological values for Definity (at 0 mm Hg) obtained here are of the same order as those obtained previously in the literature; Helfield *et al.* (2012) obtained stiffness and friction parameters to be, respectively,  $S_p = 1.95(\pm 13)$  N/m and  $S_f = 36(\pm 13) \times 10^{-8}$  Ns/m in comparison to our values of  $S_p = 2\chi = 1.73$  N/m and  $S_f = 16\pi\kappa^s = 181 \times 10^{-8}$  Ns/m.

In Fig. 7, we show how the parameters vary with overpressure increase. Figure 7(a) shows that the dilatational viscosity increases monotonically with increasing ambient overpressure. Figure 7(b) shows that the dilatational elasticity  $E_0^s$  increases with increase in ambient overpressure. The increase in elasticity is expected from the measured attenuation in Fig. 6—the peak in the attenuation curve shifts to higher frequency indicating an increased stiffness in the system. The rise in elasticity and viscosity with ambient overpressure can be understood by arguing that the enhanced

pressure decreases radius and thereby increases the density of encapsulation. Denser substrates can be expected to have higher elasticity and viscosity values. Note that Definity shell consists of DPPA and DPPC with phase transition temperatures of 67 °C and 41 °C, respectively. Therefore, at room temperature (22 °C), they are in gel state. For DPPC monolayer at gel state Vranceanu *et al.* (2007) reported an increase in dilatational elasticity and dilatational viscosity with decreasing surface area.

Note that the attenuation for Definity actually decreases with overpressure increase (Fig. 6). It is therefore somewhat puzzling to note that the dilatational viscosity increases at the same time [Fig. 7(a)]. As dilatational viscosity  $\kappa_s$  increases, the encapsulation damping  $\delta_{\text{encapsulation}}$  increases as per Eq. (12). We see in Fig. 8 that the damping coefficient  $\delta$  increases with overpressure increase. As shown before (Katiyar and Sarkar, 2012), because of the specific radius dependence (12), the encapsulation damping becomes large at smaller sizes as is also shown here. However, note that in Eq. (13), increasing  $\delta$  can either increase or decrease extinction cross-section and thereby the attenuation. Also overpressure increase leads to increased  $E^s$  which in turn increases  $\omega_0$  in Eq. (12) which may decrease attenuation. To further investigate the observed attenuation decrease, we compute extinction cross-section using the estimated properties according to Eq. (13) and plot it for two different microbubble diameters in Figs. 9(a) and 9(b). For both diameters, the extinction cross-section decreases for all frequencies with increasing ambient pressure. The overall attenuation cross-sections plotted in Fig. 5 is an integral over all diameters [see Eq. (14)] which therefore decreases. Also note that the trend of the attenuation curve in Fig. 6 is similar to those of the extinction cross-sections for individual bubbles in Fig. 9.

In order to understand the effect of the pressure on an encapsulation's rheological properties, we measured scattered response from Definity microbubble at different ambient overpressures. As we have done before, after determining the material parameters of a specific interfacial rheological model of an encapsulation, we subject the model to a validation test by comparing its prediction against a different experimental measurement—scattering. Definity microbubble was insonified at an excitation frequency of 2.25 MHz and excitation pressure of 500 kPa. In Fig. 10, the subharmonic response scattered from Definity is compared with model

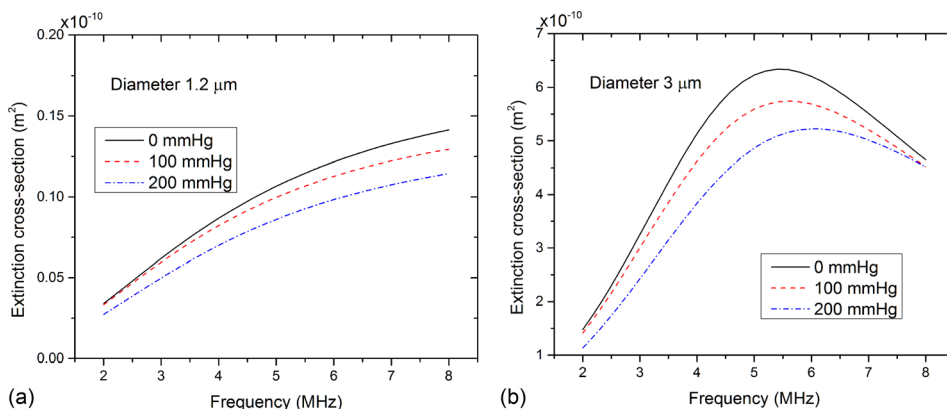


FIG. 9. (Color online) Extinction cross-sections of Definity with diameter (a) 1.2  $\mu\text{m}$  and (b) 3  $\mu\text{m}$  according to EEM model.

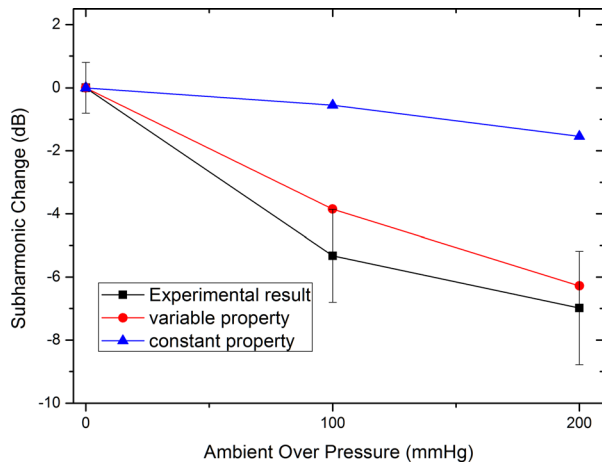


FIG. 10. (Color online) Comparison of experimentally measured subharmonic response from Definity microbubble with simulation using constant property and variable property (EEM Model).

predictions. Measured subharmonic response decreases with ambient overpressure. The model prediction that accounts for changes in encapsulation properties with changing overpressure compares favorably with the experiments. However, the model, with parameters determined at atmospheric pressure, did not. Note that for the latter case, the Eq. (1) does account for increased overpressure in the dynamics, but uses the rheological parameter values obtained by attenuation data at 0 mm Hg.

#### IV. SUMMARY AND CONCLUSION

A contrast microbubble experiences very different ambient hydrostatic pressure in different organs even under normal physiological conditions, apart from disease induced organ specific hypertension. This brief report asks the question whether ambient pressure changes affect the characteristic material properties of the encapsulation of a contrast microbubble. To answer this question, we determined material properties of Definity contrast agents—using four different interfacial rheological models. The effect of gas diffusion under overpressure leading to size decrease is accounted for. The interfacial rheological parameters for the bubbles are determined using experimentally measured ultrasound attenuation through suspensions of this agent. Different models predicted very similar values for the characteristic parameters—interfacial dilatational elasticity and viscosity. Both dilatational elasticity and dilatational viscosity show increase with increasing ambient pressure. This increase can be understood as arising from compression of the encapsulation; as the overpressure increases the microbubble decreases in size and the encapsulation increases in density. Note that in terms of the measured value of attenuation, one can also see that the peak shifts to the higher frequency indicating an overall increase in stiffness of the system, i.e., increased elasticity. Finally, we also briefly investigate the ability of the contrast agent model to predict experimentally measured scattered response. The models with pressure dependent rheological parameters matched better with measured subharmonic scattering as a function of

ambient pressure. We therefore conclude that the encapsulation rheology gets affected by the ambient pressure.

#### ACKNOWLEDGMENT

This work is partially supported by NSF Grants No. CBET-1205322, DMR-1239105 and GWU Katzen Cancer Research Center Innovative Cancer Pilot Research Award. The authors thank Dr. Jason Raymond and Professor Christy Holland for providing the size distribution data and Dr. Himanshu Shekhar for helpful discussion.

- Adam, D., Sapunar, M., and Burla, E. (2005). "On the relationship between encapsulated ultrasound contrast agent and pressure," *Ultrasound Med. Biol.* **31**, 673–686.
- Andersen, K. S., and Jensen, J. A. (2010). "Impact of acoustic pressure on ambient pressure estimation using ultrasound contrast agent," *Ultrasonics* **50**, 294–299.
- Borden, M. A., and Longo, M. L. (2002). "Dissolution behavior of lipid monolayer-coated, air-filled microbubbles: Effect of lipid hydrophobic chain length," *Langmuir* **18**, 9225–9233.
- Bouakaz, A., Frinking, P. J. A., de Jong, N., and Bom, N. (1999). "Noninvasive measurement of the hydrostatic pressure in a fluid-filled cavity based on the disappearance time of micrometer-sized free gas bubbles," *Ultrasound Med. Biol.* **25**, 1407–1415.
- Brennen, C. E. (1995). *Cavitation and Bubble Dynamics* (Oxford University Press, Oxford, UK).
- Chatterjee, D., Jain, P., and Sarkar, K. (2005a). "Ultrasound-mediated destruction of contrast microbubbles used for medical imaging and drug delivery," *Phys. Fluids* **17**, 100603.
- Chatterjee, D., and Sarkar, K. (2003). "A Newtonian rheological model for the interface of microbubble contrast agents," *Ultrasound Med. Biol.* **29**, 1749–1757.
- Chatterjee, D., Sarkar, K., Jain, P., and Schreppler, N. E. (2005b). "On the suitability of broadband attenuation measurement for characterizing contrast microbubbles," *Ultrasound Med. Biol.* **31**, 781–786.
- Church, C. C. (1995). "The effects of an elastic solid-surface layer on the radial pulsations of gas-bubbles," *J. Acoust. Soc. Am.* **97**, 1510–1521.
- D'amico, G., Pagliaro, L., and Bosch, J. (1995). "The treatment of portal hypertension: A meta-analytic review," *Hepatology* **22**, 332–354.
- deJong, N., Comet, R., and Lancee, C. T. (1994). "Higher harmonics of vibrating gas-filled microspheres. I. Simulations," *Ultrasonics* **32**, 447–453.
- deJong, N., Hoff, L., Skotland, T., and Bom, N. (1992). "Absorption and scatter of encapsulated gas filled microspheres—Theoretical considerations and some measurements," *Ultrasonics* **30**, 95–103.
- Doinikov, A. A., and Dayton, P. A. (2007). "Maxwell rheological model for lipid-shelled ultrasound microbubble contrast agents," *J. Acoust. Soc. Am.* **121**, 3331–3340.
- Epstein, P. S., and Plesset, M. S. (1950). "On the stability of gas bubbles in liquid-gas solutions," *J. Chem. Phys.* **18**, 1505–1509.
- Faez, T., Goertz, D., and De Jong, N. (2011). "Characterization of Definity (Tm) ultrasound contrast agent at frequency range of 5–15 Mhz," *Ultrasound Med. Biol.* **37**, 338–342.
- Frinking, P. J. A., Gaud, E., Brochot, J., and Arditi, M. (2010). "Subharmonic scattering of phospholipid-shell microbubbles at low acoustic pressure amplitudes," *IEEE Trans. Ultrasonics Ferroelectrics Frequency Control* **57**, 1762–1771.
- Goertz, D. E., de Jong, N., and van der Steen, A. F. W. (2007). "Attenuation and size distribution measurements of definity (TM) and manipulated definity (TM) populations," *Ultrasound Med. Biol.* **33**, 1376–1388.
- Goldberg, B. B., Raichlen, J. S., and Forsberg, F. (2001). *Ultrasound Contrast Agents: Basic Principles and Clinical Applications* (Martin Dunitz, London, UK).
- Halldorsdottir, V. G., Dave, J. K., Leodore, L. M., Eisenbrey, J. R., Park, S., Hall, A. L., Thomeniuv, K., and Forsberg, F. (2011). "Subharmonic contrast microbubble signals for noninvasive pressure estimation under static and dynamic flow conditions," *Ultrasound Imaging* **33**, 153–164.
- Helfield, B. L., Huo, X., Williams, R., and Goertz, D. E. (2012). "The effect of preactivation vial temperature on the acoustic properties of Definity (TM)," *Ultrasound Med. Biol.* **38**, 1298–1305.
- Hoff, L. (2001). *Acoustic Characterization of Contrast Agents for Medical Ultrasound Imaging* (Kluwer Academic, Norwell, MA), 208 pp.

- Hoff, L., Sontum, P. C., and Hovem, J. M. (2000). "Oscillations of polymeric microbubbles: Effect of the encapsulating shell," *J. Acoust. Soc. Am.* **107**, 2272–2280.
- Katiyar, A., and Sarkar, K. (2010). "Stability analysis of an encapsulated microbubble against gas diffusion," *J. Colloid Interface Sci.* **343**, 42–47.
- Katiyar, A., and Sarkar, K. (2011). "Excitation threshold for subharmonic generation from contrast microbubbles," *J. Acoust. Soc. Am.* **130**, 3137–3147.
- Katiyar, A., and Sarkar, K. (2012). "Effects of encapsulation damping on the excitation threshold for subharmonic generation from contrast microbubbles," *J. Acoust. Soc. Am.* **132**, 3576–3585.
- Katiyar, A., Sarkar, K., and Forsberg, F. (2011). "Modeling subharmonic response from contrast microbubbles as a function of ambient static pressure," *J. Acoust. Soc. Am.* **129**, 2325–2335.
- Katiyar, A., Sarkar, K., and Jain, P. (2009). "Effects of encapsulation elasticity on the stability of an encapsulated microbubble," *J. Colloid Interface Sci.* **336**, 519–525.
- Lawes, C. M., Vander Hoorn, S., Law, M. R., Elliott, P., MacMahon, S., and Rodgers, A. (2004). "High blood pressure," in *Comparative Quantification of Health Risks: Global and Regional Burden of Disease Attributable to Selected Major Risk Factors* (World Health Organization, Geneva, Switzerland), pp. 281–390.
- Leodore, L., Forsberg, F., and Shi, W. T. (2007). "In vitro pressure estimation obtained from subharmonic contrast microbubble signals," *IEEE Ultrasonics Symposium*, Vols. 1–6, pp. 2207–2210.
- Marmottant, P., van der Meer, S., Emmer, M., Versluis, M., de Jong, N., Hilgenfeldt, S., and Lohse, D. (2005). "A model for large amplitude oscillations of coated bubbles accounting for buckling and rupture," *J. Acoust. Soc. Am.* **118**, 3499–3505.
- Nahire, R., Haldar, M. K., Paul, S., Ambre, A. H., Meghnani, V., Layek, B., Katti, K. S., Gange, K. N., Singh, J., Sarkar, K., and Mallik, S. (2014). "Multifunctional polymersomes for cytosolic delivery of gemcitabine and doxorubicin to cancer cells," *Biomaterials* **35**, 6482–6497.
- Nahire, R., Haldar, M. K., Paul, S., Mergoum, A., Ambre, A. H., Katti, K. S., Gange, K. N., Srivastava, D. K., Sarkar, K., and Mallik, S. (2013). "Polymer-coated echogenic lipid nanoparticles with dual release triggers," *Biomacromolecules* **14**, 841–853.
- Paul, S., Katiyar, A., Sarkar, K., Chatterjee, D., Shi, W. T., and Forsberg, F. (2010). "Material characterization of the encapsulation of an ultrasound contrast microbubble and its subharmonic response: Strain-softening interfacial elasticity model," *J. Acoust. Soc. Am.* **127**, 3846–3857.
- Paul, S., Nahire, R., Mallik, S., and Sarkar, K. (2014). "Encapsulated microbubbles and echogenic liposomes for contrast ultrasound imaging and targeted drug delivery," *Comput. Mech.* **53**, 413–435.
- Paul, S., Russakow, D., Rodgers, T., Sarkar, K., Cochran, M., and Wheatley, M. A. (2013). "Determination of the interfacial rheological properties of a Poly(DL-lactic acid)-encapsulated contrast agent using in vitro attenuation and scattering," *Ultrasound Med. Biol.* **39**, 1277–1291.
- Raymond, J. L., Haworth, K. J., Bader, K. B., Radhakrishnan, K., Griffin, J. K., Huang, S. L., McPherson, D. D., and Holland, C. K. (2014). "Broadband attenuation measurements of phospholipid-shelled ultrasound contrast agents," *Ultrasound Med. Biol.* **40**, 410–421.
- Sarkar, K., Katiyar, A., and Jain, P. (2009). "Growth and dissolution of an encapsulated contrast microbubble," *Ultrasound Med. Biol.* **35**, 1385–1396.
- Sarkar, K., and Prosperetti, A. (1994). "Coherent and incoherent scattering by oceanic bubbles," *J. Acoust. Soc. Am.* **96**, 332–341.
- Sarkar, K., Shi, W. T., Chatterjee, D., and Forsberg, F. (2005). "Characterization of ultrasound contrast microbubbles using in vitro experiments and viscous and viscoelastic interface models for encapsulation," *J. Acoust. Soc. Am.* **118**, 539–550.
- Shi, W. T., Forsberg, F., Liu, J., Furuse, J., Shimizu, M., and Goldberg, B. B. (2002). "In vitro and in vivo noninvasive pressure estimation with US microbubble contrast agents," *Radiology* **225**, 410.
- Shi, W. T., Forsberg, F., Raichlen, J. S., Needleman, L., and Goldberg, B. B. (1999a). "Noninvasive pressure estimation with US microbubble contrast agents," *Radiology* **213P**, 101.
- Shi, W. T., Forsberg, F., Raichlen, J. S., Needleman, L., and Goldberg, B. B. (1999b). "Pressure dependence of subharmonic signals from contrast microbubbles," *Ultrasound Med. Biol.* **25**, 275–283.
- Simonneau, G., Robbins, I. M., Beghetti, M., Channick, R. N., Delcroix, M., Denton, C. P., Elliott, C. G., Gaine, S. P., Gladwin, M. T., and Jing, Z.-C. (2009). "Updated clinical classification of pulmonary hypertension," *J. Am. College Cardiol.* **54**, S43–S54.
- Tsiglifis, K., and Pelekasis, N. A. (2008). "Nonlinear radial oscillations of encapsulated microbubbles subject to ultrasound: The effect of membrane constitutive law," *J. Acoust. Soc. Am.* **123**, 4059–4070.
- Vranceanu, M., Winkler, K., Nirschl, H., and Leneweit, G. (2007). "Surface rheology of monolayers of phospholipids and cholesterol measured with axisymmetric drop shape analysis," *Colloid Surf. A-Physicochem. Eng. Asp.* **311**, 140–153.